Journal of Applied Physics

RESEARCH ARTICLE | JANUARY 16 2026

# Vibrational signatures of hydrogen defects in delafossite $CuMO_2$ (M = Al, Ga, In): Hybrid density-functional calculations

Aroon Ananchuensook ; Intuon Chatratin ; Anderson Janotti ; Hartwin Peelaers ; Sirichok Jungthawan ; Jiraroj T-Thienprasert ; Pakpoom Reunchan



*J. Appl. Phys.* 139, 035701 (2026)
https://doi.org/10.1063/5.0309836

Journal of Applied Physics ARTICLE pubs.aip.org/aip/jap

# Vibrational signatures of hydrogen defects in delafossite $CuMO_2$ (M = Al, Ga, In): Hybrid density-functional calculations

Cite as: J. Appl. Phys. **139**, 035701 (2026); doi: 10.1063/5.0309836
Submitted: 29 October 2025 · Accepted: 23 December 2025 ·
Published Online: 16 January 2026

View Online Export Citation CrossMark

Aroon Ananchuensook,[1,a)] Intuon Chatratin,[2] Anderson Janotti,[2] Hartwin Peelaers,[3] Sirichok Jungthawan,[4] Jiraroj T-Thienprasert,[1] and Pakpoom Reunchan[1,b)]

## AFFILIATIONS

[1]Department of Physics, Faculty of Science, Kasetsart University, Bangkok 10900, Thailand
[2]Department of Materials Science and Engineering, University of Delaware, Delaware 19716, USA
[3]Department of Physics and Astronomy, University of Kansas, Lawrence, Kansas 66045, USA
[4]School of Physics, Institute of Science, Suranaree University of Technology, Nakhon Ratchasima 30000, Thailand

[a)]**Present address:** Department of Physics and Astronomy, University of Kansas, Lawrence, KS 66045.
[b)]**Author to whom correspondence should be addressed:** pakpoom.r@ku.ac.th

## ABSTRACT

Hydrogen impurities are known to significantly influence the electronic properties of delafossite oxides $CuMO_2$ (M = Al, Ga, In) by passivating acceptor defects, thereby impacting the *p*-type conductivity of these materials. Identifying H and its configurations is, therefore, important to understand the properties of these materials. In this study, we employ hybrid density-functional theory calculations to investigate the vibrational properties of various hydrogen-related defects, including interstitial hydrogen ($H_i$), the hydrogen-copper antisite complex ($H_i$–$Cu_M$), and hydrogen-copper vacancy complexes ($H_i$–$V_{Cu}$, $2H_i$–$V_{Cu}$). Our calculations provide the first theoretical predictions of local vibrational modes associated with these defects, revealing frequencies ranging from approximately 2800 to 3800 $cm^{-1}$. These results offer valuable insights into the behavior of hydrogen in $CuMO_2$ and serve as a reference for future experimental investigations using techniques such as infrared spectroscopy. By identifying distinct vibrational signatures for different hydrogen configurations, this study lays the groundwork for defect characterization and passivation mechanisms in delafossite oxides, which are critical for optimizing their electronic and optical properties.





## I. INTRODUCTION

Hydrogen plays a crucial role in modifying the electrical properties of wide-bandgap oxide semiconductors such as ZnO, $SnO_2$, $In_2O_3$, $SrTiO_3$, and $Ga_2O_3$.[1–6] This includes *p*-type $Cu_2O$,[7,8] *p*-type CuO,[9] and *p*-type transparent metal delafossite oxides $CuMO_2$ (M = Al, Ga, In).[10] Hydrogen can be unintentionally introduced during material growth or post-processing, and its impact on the p-type conductivity is profound. In $CuMO_2$, *p*-type conductivity arises from acceptor defects, such as copper vacancies ($V_{Cu}$), which create hole carriers.[11–14] However, hydrogen can passivate these defects by forming stable neutral complexes such as $H_i$–$V_{Cu}$, effectively neutralizing the holes and reducing the overall carrier concentration. This passivation mechanism significantly degrades *p*-type performance, posing a challenge for applications in transparent electronics and optoelectronic devices that rely on robust *p*-type conductivity.

In $Cu_2O$, hydrogen bonds to oxygen and passivates $V_{Cu}$ acceptors rather than creating shallow donors.[7] Likewise, in CuO, hydrogen preferentially forms O–H bonds and passivates copper-vacancy-related acceptor states, despite the more correlated electronic structure of this oxide.[9] These similarities suggest that hydrogen can act as an effective passivating agent for copper-related acceptor centers in Cu oxides, motivating a detailed vibrational analysis of hydrogen configurations in $CuMO_2$.

In addition to affecting conductivity in oxides, hydrogen-related defects introduce local vibrational modes (LVMs) that

provide critical insights into their presence and behavior.[15] These vibrational signatures, typically in the range of 3000–3500 $cm^{-1}$, can be detected through IR and, in some cases, Raman spectroscopy.[16–18] Identifying these modes is essential for understanding how hydrogen interacts with the lattice and contributes to defect passivation. Moreover, predicting these vibrational signatures through theoretical studies offers a valuable reference for experimental efforts to detect hydrogen incorporation and characterize its impact on material properties.[19–21] Understanding the behavior of hydrogen in $CuMO_2$ is vital for controlling its detrimental effects on p-type conductivity and ensuring the long-term stability and performance of devices. The ability of hydrogen to form stable or metastable complexes under various conditions can influence the durability of $CuMO_2$-based devices. Therefore, a comprehensive understanding of hydrogen interaction with the material, particularly through vibrational analysis and defect energetics, is essential for optimizing the material properties for practical applications in transparent and optoelectronic devices.

In metal oxides such as ZnO, $SnO_2$, $In_2O_3$, and $Ga_2O_3$, hydrogen often acts as a shallow donor, contributing to n-type conductivity, or compensating holes, making *p*-type doping particularly challenging. In ZnO, infrared (IR) and Raman spectroscopy, complemented by density-functional theory (DFT) calculations, have identified multiple LVMs associated with hydrogen. For instance, Nickel and Fleischer observed six LVMs in undoped ZnO single crystals, located at 2900–3100 $cm^{-1}$,[22] which disappeared upon annealing, confirming their association with hydrogen defects. Similarly, Lavrov *et al.* identified two interstitial hydrogen-related defects in ZnO using IR absorption spectroscopy and first-principles theory, attributing specific LVMs to distinct hydrogen configurations.[23]

Hydrogen incorporation in $SnO_2$ has been extensively studied due to its impact on the material's electrical properties. Infrared (IR) spectroscopy has identified an O–H local vibrational mode (LVM) at approximately 3272 $cm^{-1}$ at 10 K, associated with a shallow donor level less than 300 meV below the conduction band.[24] This defect is stable up to about 450 °C, suggesting its potential role in persistent n-type conductivity. First-principles calculations indicate that interstitial hydrogen can easily diffuse and form stable complexes with tin vacancies, such as $(V_{Sn}–H)^{-3}$, with calculated O–H frequencies aligning well with experimental observations.[25]

In β-$Ga_2O_3$, hydrogen incorporation leads to prominent O–H stretch modes detectable via IR spectroscopy. Studies by Stavola *et al.*[26] and Weiser *et al.*[27] reported a dominant O–H vibrational mode at 3437 $cm^{-1}$, which was strongly polarized and provided insights into the microscopic properties of O–H centers in the material.

Besides, hydrogen in other wide-bandgap metal oxides, such as α-$Al_2O_3$ and $SrTiO_3$, has been extensively explored both experimentally and theoretically. T-Thienprasert *et al.* employed hybrid DFT calculations to investigate the behavior of hydrogen in α-$Al_2O_3$. Their studies revealed that hydrogen can form stable complexes with intrinsic defects, such as Al vacancies, leading to the formation of O–H bonds detectable by infrared spectroscopy.[19] Hydrogen's interaction with intrinsic point defects in $SrTiO_3$ has also been extensively investigated.[28,29] It has been demonstrated that hydrogen can occupy interstitial sites or form complexes with Ti vacancies, leading to various local vibrational modes (LVMs).[20] These theoretical predictions align well with experimental observations,[30,31] providing a comprehensive understanding of hydrogen's behavior in $SrTiO_3$. These findings illustrate the critical role of LVMs in identifying and understanding hydrogen-related defects in oxide semiconductors.

Despite the substantial work on hydrogen in oxides, there is a noticeable gap in the literature regarding delafossite oxides, such as $CuMO_2$ (M = Al, Ga, In). While these materials are promising candidates for transparent *p*-type semiconductors, very few studies have explored the role of hydrogen in passivating acceptor defects such as copper vacancies ($V_{Cu}$).[10] Most of the existing research on $CuMO_2$ has focused on its optical properties, structural characteristics, and intrinsic defect chemistry.[32] However, the specific interaction between hydrogen and these materials still needs to be addressed. Additionally, there are no experimental reports of hydrogen-related vibrational modes in $CuMO_2$, leaving a critical gap in understanding how hydrogen incorporation affects their *p*-type conductivity.

This lack of experimental data and theoretical investigations into the behavior of hydrogen in $CuMO_2$ presents an opportunity for significant advances. Addressing this gap is crucial for developing transparent *p*-type semiconductors with optimized electrical performance. By leveraging hybrid DFT calculations, this study aims to predict the vibrational signatures of hydrogen-related defects in $CuMO_2$ and provide theoretical benchmarks for future experimental efforts. Understanding the passivation mechanisms and vibrational properties of hydrogen in $CuMO_2$ will help bridge the gap between theory and experiment, guiding the design of more efficient and stable materials for transparent electronics and optoelectronics.

In this work, we employ hybrid density-functional calculations to predict the local vibrational mode (LVM) frequencies of key hydrogen-related defects in delafossite $CuMO_2$ (M = Al, Ga, In), specifically interstitial hydrogen ($H_i$), hydrogen-copper antisite complexes ($H_i–Cu_M$), and hydrogen-copper vacancy complexes ($H_i–V_{Cu}$, $2H_i–V_{Cu}$). Each defect type exhibits distinct vibrational signatures with calculated frequencies ranging from approximately 2800 to 3800 $cm^{-1}$, providing precise theoretical benchmarks for their experimental identification via IR spectroscopy. Our results demonstrate that the vibrational frequencies of isolated interstitial hydrogen ($H_i$) are generally lower due to its weaker local bonding environment and longer O–H bond lengths. In contrast, complexes such as $H_i–V_{Cu}$ and, in particular, $2H_i–V_{Cu}$ exhibit higher frequencies, reflecting stronger and more rigid local bonding configurations.

These findings offer theoretical predictions for the vibrational spectra of hydrogen in $CuMO_2$ and provide a framework for understanding how different hydrogen-related defects influence the material properties. The results have significant implications for the detection and characterization of hydrogen in $CuMO_2$ using IR spectroscopy, serving as a reference for future experimental studies aimed at optimizing the *p*-type conductivity of these materials through controlled hydrogen and defect incorporation.

## II. COMPUTATIONAL METHOD

We used density-functional theory (DFT), and the Heyd–Scuseria–Ernzerhof (HSE) screened hybrid functional;[33] we

**TABLE I.** Chemical potentials for the stable growth of $CuMO_2$ at the experimental conditions. Units of $\tilde{\mu}_{Cu}$, $\tilde{\mu}_M$, and $\tilde{\mu}_O$ are in eV.

| | $CuAlO_2$ | $CuGaO_2$ | $CuInO_2$ |
|---|---|---|---|
| $\tilde{\mu}_{Cu}$, $\tilde{\mu}_M$, and $\tilde{\mu}_O$ | −0.13, −5.90, −1.45 | −0.13, −2.90, −1.45 | −0.08, −2.10, −1.45 |

treated Cu $3d^{10}4s^1$, Al $3s^23p^163s^23p^1$ Ga $4s^24p^1$, In $5s^25p^1$, O $2s^22p^4$, and the H $1s^1$ as valence electrons through the projector augmented-wave method[34] as implemented in the VASP code.[35,36] The plane-wave basis cutoff was set at 400 eV. We used 25% of Hartree–Fock (HF) exchange with a screening length parameter of 0.2 $Å^{-1}$. We used a 108-atom supercell using a $3 \times 3 \times 1$ repetition of the 12-atom conventional cell of $CuMO_2$ to model H-related impurities and calculate their vibrational frequencies. Integration over the Brillouin Zone employed a special $k$ point at (¼, ¼, ¼). The formation energy of H-related defects, for instance, the $H_i$–$V_{Cu}$ complex in charge state $q$, is given by[37]

$$E^f[(H_i - V_{Cu})^q] = E_{tot}((H_i - V_{Cu})^q) - E_{tot}(CuMO_2) + \mu_{Cu} - \mu_H + q(\varepsilon_F + E_v) + \Delta^q, \quad (1)$$

where $E_{tot}((H_i - V_{Cu})^q)$ is the total energy of the supercell containing the $H_i$–$V_{Cu}$ complex in charge state $q$ and $E_{tot}(CuMO_2)$ is the total energy of a perfect crystal in the same supercell. For a charged $H_i$–$V_{Cu}$, electrons will be added to or removed from the Fermi level ($\varepsilon_F$), which is referenced to the valence-band maximum (VBM, $E_v$) of the host materials. The chemical potential of Cu was referenced to the total energy per atom of the copper bulk ($\mu_{Cu} = \tilde{\mu}_{Cu} + E_{tot}[Cu]$). The chemical potential of hydrogen, $\tilde{\mu}_H$, is limited by the formation of $H_2O$, i.e., $\tilde{\mu}_H = [\Delta H_f(H_2O) - \tilde{\mu}_O]/2$. The detailed analysis for constructing the thermodynamic equilibrium chemical potential diagram of $CuMO_2$ can be found in Ref. 10. The last term $\Delta^q$ represents the correction for the effects of the finite size of the supercell containing charged defects.[10,38] In the present work, the oxygen chemical potential was chosen to represent the effective growth environment during pulsed laser deposition (PLD) of $CuMO_2$ thin films at 700 °C under $O_2$ pressure ranging from $\sim 10^{-5}$ to $10^{-4}$ atm.[10] These conditions yield an oxygen chemical potential of about −1.45 eV (see the supplementary material for details). Using this O chemical potential, we also estimated the chemical potential of Cu and M metals, as shown in Fig. S1 in the supplementary material, with the values in Table I.

The local vibrational modes (LVMs) associated with hydrogen-related defects were determined by constructing the potential energy curve (PEC) along the vibrational coordinate. Following established approaches for vibrational mode analysis,[39–43] the hydrogen atom was displaced incrementally along its vibrational axis while all other atoms were fixed at their equilibrium positions. This approximation is justified by the significant mass difference between hydrogen and the host atoms, ensuring that the vibrational mode is predominantly localized on the hydrogen atom. The potential energy curve $V(x)$ was fitted to a fourth-order polynomial to account for anharmonic contributions,

$$V(x) = \frac{k}{2}x^2 + \alpha x^3 + \beta x^4, \quad (2)$$

where $x$ is the displacement from the equilibrium position, $k$ is the harmonic force constant, and $\alpha$ and $\beta$ are coefficients representing the cubic and quartic anharmonic terms, respectively. The harmonic frequency $\tilde{\omega}_h$ was obtained using $\tilde{\omega}_h = \sqrt{\frac{k}{\mu}}$, where $\mu$ is the reduced mass of the hydrogen-host atom system defined by $\frac{1}{\mu} = \frac{1}{m_H} + \frac{1}{m_O}$; $m_H$ and $m_O$ are the atomic masses of O and H, respectively. We, thus, obtain the stretch frequency as

$$\tilde{\omega} = \tilde{\omega}_h + \tilde{\omega}_{anh} = \sqrt{\frac{k}{\mu}} - 3\frac{\hbar}{\mu}\left(\frac{5\alpha^2}{2k^2} - \frac{\beta}{k}\right), \quad (3)$$

where $\tilde{\omega}_{anh}$ represents the anharmonic correction.

## III. RESULTS AND DISCUSSION

Figure 1 illustrates the calculated formation energies of critical hydrogen-related defects in $CuMO_2$ (M = Al, Ga, In) at experimentally relevant growth conditions (700 °C, $O_2$ pressure $\sim 10^{-5}$–$10^{-4}$ atm) using the chemical potentials listed in Table I. The defects considered include isolated interstitial hydrogen ($H_i$), hydrogen-copper antisite complexes ($H_i$–$Cu_M$), and hydrogen-copper vacancy complexes ($H_i$–$V_{Cu}$, $2H_i$–$V_{Cu}$). In all three systems, $CuAlO_2$, $CuGaO_2$, and $CuInO_2$, the $H_i$–$V_{Cu}$ complex (blue line) emerges as the most stable defect configuration across the entire range of Fermi level. It has a significantly lower formation energy than isolated interstitial hydrogen ($H_i$, red line) and other complexes, suggesting that it will dominate hydrogen-related defect populations under typical synthesis conditions. As previously reported in Ref. 10, the dissociation temperature was estimated using a transition-state-theory model, where the dissociation barrier is approximated as the sum of the binding energy and the hydrogen migration barrier. Using 2.5–2.7 eV yields dissociation temperatures of approximately 600–700 °C (≈870–970 K). This high thermodynamic stability of the complex further underscores its critical role in defect passivation and reduction of $p$-type conductivity.

The $2H_i$–$V_{Cu}$ complexes (black line), where two hydrogen atoms occupy copper vacancy sites, have relatively low formation energies, particularly notable in $CuGaO_2$ and $CuInO_2$ at lower Fermi levels. The binding energies of the $2H_i$–$V_{Cu}$ complexes in the +1 charge state range from approximately 0.95 to 1.37 eV; the detailed formalism and binding energy values for all relevant defect complexes are explicitly outlined in our previous work,[10] which examines the same hydrogen-vacancy complexes using identical computational settings. However, these complexes are energetically less favorable compared to the single hydrogen-vacancy complex

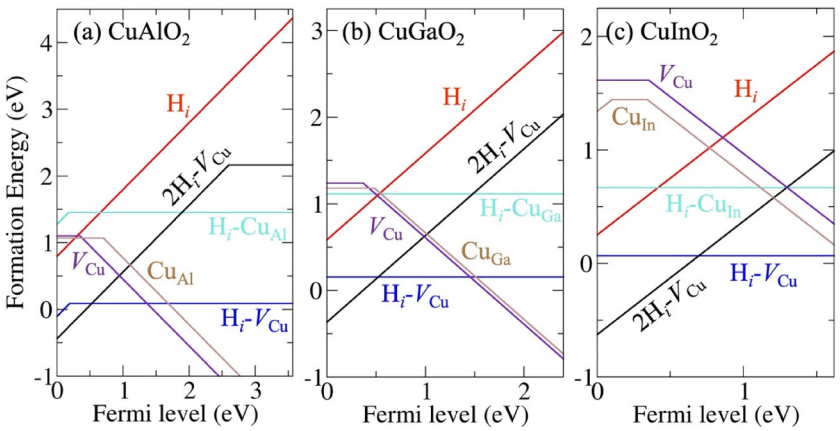


**FIG. 1.** Formation energies for H impurities and related native defects in (a) $CuAlO_2$, (b) $CuGaO_2$, and (c) $CuInO_2$ as a function of Fermi level under the experimental condition.

($H_i$–$V_{Cu}$) at higher Fermi levels, highlighting a thermodynamic preference for the formation of the single-hydrogen complex under typical growth conditions. On the other hand, the formation energy of the hydrogen-copper antisite complexes ($H_i$–$Cu_M$, cyan line) is comparatively higher across all systems, indicating lower stability and reduced likelihood of formation. This finding suggests that $H_i$–$Cu_M$ complexes are expected to have relatively minor roles in passivation compared to vacancy-related complexes. Although hydrogen is not intentionally introduced, it can be incorporated into $CuMO_2$ via residual $H_2O$ or $H_2$ in growth environments, hydrogen impurities in targets or substrates, and post-growth exposure to ambient air, providing realistic pathways for the formation of the hydrogen–defect complexes predicted here.

To validate the accuracy of the vibrational frequency calculations and quantify systematic deviations due to the choice of method and functional, we first computed the symmetric stretch mode of the $H_2O$ molecule using both the potential energy curve (PEC) approach and the finite-difference (FD) method, as shown in Table II. The LDA calculations were included solely for comparison with established benchmarks,[41] while the HSE functional was used for all reported results in this work. While the PEC approach allows anharmonic corrections, the FD method yields only harmonic frequencies. Based on comparisons with experimental data, we determined empirical correction terms as the difference between the calculations and the experiments: $\Delta\omega_{ER} = -125\ cm^{-1}$ for PEC-based frequencies and $-241\ cm^{-1}$ for FD-based frequencies. For isolated hydrogen-related defects such as $H_i$, $H_i$–$V_{Cu}$, and $H_i$–$Cu_M$, where hydrogen vibrates largely independently, we used the PEC approach combined with the anharmonic correction and applied $\Delta\omega_{ER} = -125\ cm^{-1}$ to the calculated frequencies. However, for complexes like $2H_i$–$V_{Cu}$, the vibrational behavior involves two coupled hydrogen oscillators. Using the full dynamical matrix constructed via the finite-difference method, our calculations showed that the two hydrogen atoms couple into symmetric and antisymmetric stretch modes. These modes were identified from the eigenvectors of the dynamical matrix, based on the relative phase of the hydrogen displacements along the O–H bonds. Notably, only the antisymmetric mode is IR active.[27] Since anharmonic PEC fitting is inappropriate for coupled modes, we applied the FD-based correction of $\Delta\omega_{ER} = -241$ to the $2H_i$–$V_{Cu}$ complex. To illustrate the application of our vibrational analysis method to hydrogen-related defects in $CuMO_2$, we present the potential energy curves and bonding environment for $H_i$ and the $H_i$–$V_{Cu}$ in $CuAlO_2$ in Fig. 2.

Figure 2 presents the calculated potential energy curves (PECs) and electron localization function (ELF) analyses for



**TABLE II.** The calculated symmetric stretch mode frequencies of $H_2O$ obtained by the approach in this work (PEC) and the finite difference (FD) by constructing a full dynamical matrix and the O–H bond length ($d_{O-H}$). $\tilde{\omega}_h$ and $\tilde{\omega}_{anh}$ are the harmonic frequency and the anharmonic correction. $\Delta\omega_{ER}$ is the empirical correction defined as $\Delta\omega_{ER} = \tilde{\omega}_{exp} - \tilde{\omega}$. The unit of frequency is $cm^{-1}$. The experimental values are also listed.

| Method | $d_{O-H}$ (Å) | $\tilde{\omega}_h$ | $\tilde{\omega}_{anh}$ | $\tilde{\omega}$ | $\Delta\omega_{ER}$ |
|---|---|---|---|---|---|
| PEC (HSE)[a] | 0.973 | 3714 | 68 | 3782 | −125 |
| PEC (LDA)[a] | 0.973 | 3732 | −134 | 3598 | 59 |
| PEC (LDA)[b] | 0.975 | 3815 | −257 | 3559 | 98 |
| FD (HSE)[a] | 0.973 | 3898 | | 3898 | −241 |
| | | | | $\tilde{\omega}_{exp}$ | |
| Expt.[c] | 0.957 | | | 3657 | |

[a]This work.
[b]Reference 41.
[c]Reference 44.

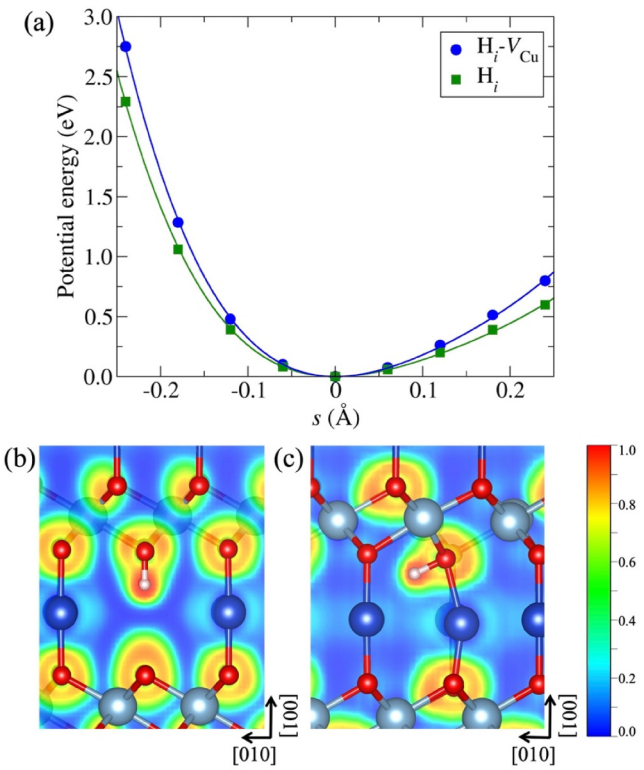


**FIG. 2.** (a) Potential energy curves for O–H bond displacement in $H_i$ and the $H_i$–$V_{Cu}$ in $CuAlO_2$. The slightly steeper curvature for $H_i$–$V_{Cu}$ indicates a stronger local bonding environment. (b) and (c) Electron localization function (ELF) plots for $H_i$–$V_{Cu}$ and $H_i$, respectively, illustrating the spatial distribution of electron density around the hydrogen site. The ELF values are shown on a dimensionless scale ranging from 0 (blue) to 1 (red).

hydrogen-related defects in $CuAlO_2$. Panel (a) compares the potential energy as a function of the O–H bond displacement for $H_i$ and the $H_i$–$V_{Cu}$. Both defects exhibit approximately harmonic potential wells near the equilibrium positions, with slight deviations indicative of anharmonicity. The potential curve for $H_i$–$V_{Cu}$ (blue circles) is slightly narrower and steeper than that of isolated $H_i$ (green squares), suggesting a stronger, more rigid local bonding environment around the hydrogen atom in the vacancy complex.

Panels (b) and (c) show the ELF plots for the $H_i$–$V_{Cu}$ complex and isolated $H_i$, respectively. The ELF analysis visually confirms differences in local bonding characteristics between the two configurations. In the $H_i$–$V_{Cu}$ complex, panel (b), significant electron localization around the hydrogen and adjacent oxygen atoms is clearly evident, reflecting robust O–H bonding and consistent with the higher vibrational frequencies observed. Conversely, isolated interstitial hydrogen, panel (c) exhibits comparatively less localized electron density around the hydrogen atom, consistent with slightly weaker bonding and lower vibrational frequencies. Although this figure illustrates results specifically for $CuAlO_2$, we expect qualitatively similar behavior for analogous hydrogen-related defects in $CuGaO_2$ and $CuInO_2$, given their comparable crystal structures and bonding characteristics.

**TABLE III.** Stretch mode frequencies for hydrogen-related defects $\tilde{\omega}_h$, $\tilde{\omega}_{anh}$, and $\tilde{\omega}$ defined in Eq. (3) for $CuAlO_2$, $CuGaO_2$, and $CuInO_2$, and the corrected frequency $\omega$. The unit is $cm^{-1}$. The calculated O–H bond lengths are also listed.

| Defects | $q$ | $d_{O-H}$ (Å) | $\tilde{\omega}_h$ | $\tilde{\omega}_{anh}$ | $\omega(\tilde{\omega})$ |
|---|---|---|---|---|---|
| | | $CuAlO_2$ | | | |
| $H_i$ | 1+ | 0.992 | 3296 | −381 | 2789 (2915) |
| $H_i$–$V_{Cu}$ | 1+ | 0.970 | 3712 | −295 | 3292 (3417) |
| | 0 | 0.971 | 3699 | −302 | 3272 (3397) |
| $H_i$–$Cu_{Al}$ | 1+ | 0.979 | 3507 | −354 | 3028 (3152) |
| | 0 | 0.979 | 3507 | −357 | 3025 (3150) |
| $2H_i$–$V_{Cu}$ (sym) | 1+ | 0.958 | 3958 | | 3776 |
| $2H_i$–$V_{Cu}$ (asym) | | | 3985 | | 3804 |
| | | $CuGaO_2$ | | | |
| $H_i$ | 1+ | 0.987 | 3573 | −336 | 3111 (3237) |
| $H_i$–$V_{Cu}$ | 0 | 0.972 | 3844 | −292 | 3427 (3552) |
| $H_i$–$Cu_{Ga}$ | 0 | 0.977 | 3697 | −329 | 3249 (3368) |
| $2H_i$–$V_{Cu}$ (sym) | 1+ | 0.959 | 3958 | | 3776 |
| $2H_i$–$V_{Cu}$ (asym) | | | 3985 | | 3804 |
| | | $CuInO_2$ | | | |
| $H_i$ | 1+ | 0.984 | 3474 | −337 | 3012 (3137) |
| $H_i$–$V_{Cu}$ | 0 | 0.974 | 3691 | −313 | 3254 (3379) |
| $H_i$–$Cu_{In}$ | 0 | 0.973 | 3627 | −314 | 3188 (3313) |
| $2H_i$–$V_{Cu}$ (sym) | 1+ | 0.959 | 3959 | | 3778 |
| $2H_i$–$V_{Cu}$ (asym) | | | 3977 | | 3796 |

Table III displays the calculated O–H bond lengths and vibrational stretch-mode frequencies for hydrogen-related defects in $CuAlO_2$, $CuGaO_2$, and $CuInO_2$. In all three compounds, a clear correlation is observed between the O–H bond length and the vibrational frequency, indicating that hydrogen modes are sensitive to local bonding environments. For $H_i$, the longest O–H bond lengths (0.984–0.992 Å) correspond to the lowest corrected vibrational frequencies, ranging from 2789 $cm^{-1}$ in $CuAlO_2$ to 3111 $cm^{-1}$ in $CuGaO_2$. This trend reflects weak hydrogen binding in the interstitial site and is consistent with the expectation that longer bonds lead to softer vibrational modes.

In contrast, $H_i$–$V_{Cu}$ displays shorter O–H bonds (≈0.970–0.974 Å) and higher vibrational frequencies. Corrected frequencies of 3254 $cm^{-1}$ ($CuInO_2$), 3272 to 3292 $cm^{-1}$ ($CuAlO_2$), and 3427 $cm^{-1}$ ($CuGaO_2$) clearly indicate stronger hydrogen–lattice interactions when hydrogen binds near a copper vacancy. These values demonstrate that vacancy-related hydrogen defects are both more stable and spectroscopically distinguishable from isolated interstitials. The antisite complexes ($H_i$–$Cu_M$, with M = Al, Ga, In) yield intermediate values, with O–H bond lengths ranging from 0.973 to 0.979 Å and corrected vibrational frequencies between 3150 and 3368 $cm^{-1}$. Their positions between $H_i$ and $H_i$–$V_{Cu}$ confirm that antisite-related defects create moderately strong hydrogen bonding environments.

Finally, $2H_i$–$V_{Cu}$ consistently exhibits the highest vibrational modes. In the relaxed $2H_i$–$V_{Cu}$ configuration, the two hydrogen atoms are separated by approximately 1.80–1.83 Å, indicating a

compact geometry that facilitates strong vibrational coupling. The symmetric and antisymmetric stretches occur within a narrow range of 3776 to 3804 $cm^{-1}$ across all three materials, indicating strong hydrogen–hydrogen coupling and offering a reliable vibrational fingerprint for these complexes regardless of the M cation chosen. Overall, the order of vibrational frequencies remains consistent across $CuAlO_2$, $CuGaO_2$, and $CuInO_2$: $H_i < H_i–Cu_M < H_i–V_{Cu} < 2H_i–V_{Cu}$. This consistent pattern confirms that hydrogen-related vibrational signatures are primarily determined by local bonding geometry rather than overall lattice chemistry variations. The narrow frequency ranges associated with each defect type also suggest that experimental IR spectroscopy can reliably distinguish isolated, vacancy-related, and multi-hydrogen complexes, providing valuable benchmarks for identifying hydrogen incorporation mechanisms in *p*-type delafossite oxides.

In addition to identifying local vibrational modes (LVMs) at ambient conditions, pressure-dependent infrared (IR) spectroscopy offers a powerful method for distinguishing between different hydrogen-related defects in oxide materials. The sensitivity of the vibrational frequency shifts (dω/dP) under hydrostatic pressure reflects variations in the local bonding environment around the hydrogen atoms. Defects with loosely bound hydrogen, such as isolated interstitial hydrogen ($H_i$), typically exhibit larger negative frequency shifts under increased pressure, due to greater local compressibility and bond weakening. In contrast, tightly bonded hydrogen complexes, like $2H_i–V_{Cu}$, generally display more minor negative or even positive frequency shifts owing to their more rigid and less compressible local structures. Previous experimental studies using pressure-dependent IR spectroscopy on hydrogen-related defects in materials such as ZnO[45,46] and $SnO_2$[25] have demonstrated that these pressure shifts can distinctly characterize defect types. Applying similar methodologies to $CuMO_2$ materials will provide an experimental basis for clearly distinguishing $H_i$, $2H_i–V_{Cu}$, and $2H_i–V_{Cu}$ defects, facilitating targeted identification and improved control of defect chemistry in these transparent oxide semiconductors.

Although direct experimental measurements of hydrogen-related vibrational modes in $CuMO_2$ have not yet been reported, previous infrared (IR) spectroscopy studies on hydrogen defects in other oxide semiconductors, such as ZnO, $SnO_2$, $In_2O_3$, and $Ga_2O_3$, have successfully identified local vibrational modes (LVMs) in the frequency range of approximately 2800–3600 $cm^{-1}$.[18,23,25–27,46–48] These findings demonstrate the practical feasibility of detecting hydrogen configurations via IR-active modes. Our theoretical predictions, thus, serve as essential benchmarks, providing precise targets for future experimental investigations. Such experimental validation in $CuMO_2$ will confirm the presence and nature of hydrogen-related defects and provide valuable insights into defect formation and passivation mechanisms, thereby facilitating improved control over *p*-type conductivity and overall performance of these promising transparent oxide materials.

## IV. CONCLUSION

In conclusion, our comprehensive theoretical analysis using hybrid density-functional calculations has identified and characterized the vibrational signatures of hydrogen-related defects in $CuMO_2$ (M = Al, Ga, In). We established the relative stability and vibrational fingerprints of defects such as interstitial hydrogen ($H_i$), hydrogen-copper vacancy complexes ($H_i–V_{Cu}$, $2H_i–V_{Cu}$), and hydrogen-copper antisite complexes ($H_i–Cu_M$). Through detailed analyses of potential energy curves and anharmonic frequency corrections, we provided accurate theoretical benchmarks for future experimental validation. These results offer critical insights into the defect chemistry of delafossite oxides and highlight specific experimental strategies, including pressure-dependent infrared spectroscopy, for detecting and distinguishing hydrogen-related defects. Ultimately, this work paves the way for improved defect engineering and optimized *p*-type conductivity in transparent oxide semiconductors, enabling advances in transparent electronics and optoelectronic devices.

## SUPPLEMENTARY MATERIAL

See the supplementary material for detailed calculations: (1) for the chemical potentials of oxygen under the experimental condition and chemical potential diagram of $CuMO_2$, (2) the binding energies of the defect complexes, and (3) the reduced mass of the $H_2O$ molecule.

## ACKNOWLEDGMENTS

This work was supported by the Kasetsart Research and Development Institute (KURDI) through Fundamental Funds (FF (KU)55.69). P.R. acknowledges the NSRF via the Program Management Unit for Human Resources & Institutional Development, Research, and Innovation (Grant No. B39G670019). We thank the NSTDA Supercomputer Center (ThaiSC) for providing computing resources for this work. A.J. acknowledges support from NSF through the UD-CHARM University of Delaware Materials Research Science and Engineering Center (MRSEC) (Grant No. DMR-2011824).



## AUTHOR DECLARATIONS

### Conflict of Interest

The authors have no conflicts to disclose.

### Author Contributions

**Aroon Ananchuensook:** Data curation (equal); Investigation (equal); Methodology (equal); Visualization (equal); Writing – original draft (equal); Writing – review & editing (equal). **Intuon Chatratin:** Investigation (supporting); Writing – review & editing (supporting). **Anderson Janotti:** Supervision (equal); Writing – review & editing (equal). **Hartwin Peelaers:** Writing – review & editing (equal). **Sirichok Jungthawan:** Writing – review & editing (supporting). **Jiraroj T-Thienprasert:** Methodology (equal); Writing – review & editing (supporting). **Pakpoom Reunchan:** Conceptualization (equal); Funding acquisition (equal); Investigation (equal); Supervision (equal); Writing – original draft (equal); Writing – review & editing (equal).

## DATA AVAILABILITY

The data that support the findings of this study are available from the corresponding author upon reasonable request.

## REFERENCES


[1]S. K. Estreicher, Mater. Sci. Eng. R: Rep. **14**(7–8), 319–412 (1995).
[2]C. G. Van de Walle, Phys. Rev. Lett. **85**(5), 1012 (2000).
[3]C. G. Van de Walle and J. Neugebauer, Annu. Rev. Mater. Res. **36**, 179–198 (2006).
[4]P. D. C. King, R. L. Lichti, Y. G. Celebi, J. M. Gil, R. C. Vilão, H. V. Alberto, J. Piroto Duarte, D. J. Payne, R. G. Egdell, I. McKenzie, C. F. McConville, S. F. J. Cox, and T. D. Veal, Phys. Rev. B **80**(8), 081201 (2009).
[5]S. Limpijumnong, P. Reunchan, A. Janotti, and C. G. Van de Walle, Phys. Rev. B **80**(19), 193202 (2009).
[6]P. Reunchan, N. Umezawa, A. Janotti, J. T-Thienprasert, and S. Limpijumnong, Phys. Rev. B **95**(20), 205204 (2017).
[7]D. O. Scanlon and G. W. Watson, Phys. Rev. Lett. **106**(18), 186403 (2011).
[8]K. Biswas, M. H. Du, J. T-Thienprasert, S. Limpijumnong, and D. J. Singh, Phys. Rev. Lett. **108**(21), 219703 (2012).
[9]A. Živković and N. H. de Leeuw, Phys. Rev. Mater. **4**(7), 074606 (2020).
[10]A. Ananchuensook, I. Chatratin, A. Janotti, T. Watcharatharapong, J. T-Thienprasert, A. Boonchun, S. Jungthawan, and P. Reunchan, J. Appl. Phys. **135**(18), 185705 (2024).
[11]D. O. Scanlon and G. W. Watson, J. Phys. Chem. Lett. **1**(21), 3195–3199 (2010).
[12]H. Kawazoe, M. Yasukawa, H. Hyodo, M. Kurita, H. Yanagi, and H. Hosono, Nature **389**(6654), 939 (1997).
[13]K. Ueda, T. Hase, H. Yanagi, H. Kawazoe, H. Hosono, H. Ohta, M. Orita, and M. Hirano, J. Appl. Phys. **89**(3), 1790–1793 (2001).
[14]H. Yanagi, T. Hase, S. Ibuki, K. Ueda, and H. Hosono, Appl. Phys. Lett. **78**(11), 1583–1585 (2001).
[15]M. D. McCluskey, J. Appl. Phys. **87**(8), 3593–3617 (2000).
[16]E. V. Lavrov, J. Weber, L. Huang, and B. B. Nielsen, Phys. Rev. B **64**(3), 035204 (2001).
[17]E. V. Lavrov, I. Chaplygin, F. Herklotz, and V. V. Melnikov, Phys. Status Solidi B **258**(8), 2100171 (2021).
[18]E. V. Lavrov, F. Börrnert, and J. Weber, Phys. Rev. B **71**(3), 035205 (2005).
[19]J. T-Thienprasert, A. Boonchun, P. Reunchan, and S. Limpijumnong, Phys. Rev. B **95**(13), 134103 (2017).
[20]J. T-Thienprasert, I. Fongkaew, D. J. Singh, M. H. Du, and S. Limpijumnong, Phys. Rev. B **85**(12), 125205 (2012).
[21]S. Limpijumnong, P. Reunchan, A. Janotti, and C. G. Van de Walle, Phys. Rev. B **77**(19), 195209 (2008).
[22]N. H. Nickel and K. Fleischer, Phys. Rev. Lett. **90**(19), 197402 (2003).
[23]E. V. Lavrov, J. Weber, F. Börrnert, C. G. Van de Walle, and R. Helbig, Phys. Rev. B **66**(16), 165205 (2002).
[24]F. Herklotz, I. Chaplygin, E. V. Lavrov, and V. F. Agekyan, Appl. Phys. Lett. **114**(15), 152103 (2019).
[25]F. Herklotz, E. V. Lavrov, V. V. Melnikov, Z. Galazka, and V. F. Agekyan, Phys. Rev. B **108**(20), 205204 (2023).
[26]M. Stavola, W. B. Fowler, A. Portoff, A. Venzie, E. R. Glaser, and S. J. Pearton, J. Appl. Phys. **135**(10), 101101 (2024).
[27]P. Weiser, M. Stavola, W. B. Fowler, Y. Qin, and S. Pearton, Appl. Phys. Lett. **112**(23), 232104 (2018).
[28]J. B. Varley, H. Peelaers, A. Janotti, and C. G. Van de Walle, J. Phys.: Condens. Matter **23**(33), 334212 (2011).
[29]J. B. Varley, A. Janotti, and C. G. Van de Walle, Phys. Rev. B **89**(7), 075202 (2014).
[30]G. Weber, S. Kapphan, and M. Wöhlecke, Phys. Rev. B **34**(12), 8406–8417 (1986).
[31]M. C. Tarun and M. D. McCluskey, J. Appl. Phys. **109**(6), 063706 (2011).
[32]T. Gake, Y. Kumagai, A. Takahashi, and F. Oba, Phys. Rev. Mater. **5**(10), 104602 (2021).
[33]J. Heyd, G. E. Scuseria, and M. Ernzerhof, J. Chem. Phys. **118**(18), 8207–8215 (2003).
[34]P. E. Blöchl, Phys. Rev. B **50**(24), 17953–17979 (1994).
[35]G. Kresse and J. Hafner, Phys. Rev. B **47**(1), 558–561 (1993).
[36]G. Kresse and J. Furthmüller, Comput. Mater. Sci. **6**(1), 15–50 (1996).
[37]C. Freysoldt, B. Grabowski, T. Hickel, J. Neugebauer, G. Kresse, A. Janotti, and C. G. Van de Walle, Rev. Mod. Phys. **86**(1), 253–305 (2014).
[38]C. Freysoldt, J. Neugebauer, and C. G. Van de Walle, Phys. Rev. Lett. **102**(1), 016402 (2009).
[39]S. Limpijumnong and S. B. Zhang, Appl. Phys. Lett. **86**(15), 151910 (2005).
[40]S. Limpijumnong, J. E. Northrup, and C. G. Van de Walle, Phys. Rev. B **68**(7), 075206 (2003).
[41]S. Limpijumnong, MRS Online Proc. Libr. **813**(1), 361–372 (2004).
[42]C. G. Van de Walle and J. P. Goss, Mater. Sci. Eng. B **58**(1–2), 17–23 (1999).
[43]C. G. Van de Walle, Phys. Rev. B **56**(16), R10020–R10023 (1997).
[44]T. Shimanouchi, *Tables of Molecular Vibrational Frequencies, Consolidated Volume 1, NSRDS NBS-39* (U.S. Government Printing Office, Washington, DC, 1972).
[45]E. V. Lavrov, F. Herklotz, and J. Weber, Phys. Rev. B **79**(16), 165210 (2009).
[46]E. V. Lavrov and J. Weber, Phys. Rev. B **73**(3), 035208 (2006).
[47]P. Weiser, Y. Qin, W. Yin, M. Stavola, W. B. Fowler, and L. A. Boatner, Appl. Phys. Lett. **109**(20), 202105 (2016).
[48]Y. Qin, M. Stavola, W. B. Fowler, P. Weiser, and S. J. Pearton, ECS J. Solid State Sci. Technol. **8**(7), Q3103 (2019).